

Article

A State of Charge Estimation Approach for Lithium-Ion Batteries Based on the Optimized Metabolic EGM(1,1) Algorithm

Qiang Sun ^{1,2,*} , Shasha Wang ³, Shuang Gao ², Haiying Lv ^{1,*}, Jianghao Liu ¹, Li Wang ¹, Jifei Du ⁴ and Kexin Wei ²¹ College of Engineering and Technology, Tianjin Agricultural University, Tianjin 300392, China² Key Laboratory of the Ministry of Education on Smart Power Grids, Tianjin University, Tianjin 300072, China³ Research and Development Centre, Beijing Electric Vehicle Co., Ltd., Beijing 100176, China⁴ National Active Distribution Network Technology Research Center (NANTEC), Beijing Jiaotong University, Beijing 100044, China

* Correspondence: sunqiang@tju.edu.cn (Q.S.); tjau2018@tjau.edu.cn (H.L.)

Abstract: The accurate estimation of the state of charge (SOC) for lithium-ion batteries' performance prediction and durability evaluation is of paramount importance, which is significant to ensure reliability and stability for electric vehicles. The SOC estimation approaches based on big data collection and offline adjustment could result in imprecision for SOC estimation under various driving conditions at different temperatures. In the traditional GM(1,1), the initialization condition and the identifying parameter could not be changed as soon as they are confirmed. Aiming at the requirements of battery SOC estimation with non-linear characteristics of a dynamic battery system, the paper presents a method of battery state estimation based on Metabolic Even GM(1,1) to expand battery state data and introduce temperature factors in the estimation process to make SOC estimation more accurate. The latest information data used in the optimized rolling model is introduced through the data cycle updating. The experimental results show that the optimized MEGM(1,1) effectively considers the influence of initial data, and has higher accuracy than the traditional GM(1,1) model in the application of data expansion. Furthermore, it could effectively solve the problem of incomplete battery information and battery capacity fluctuation, and the dynamic performance is satisfactory to meet the requirements of fast convergence. The SOC estimation based on the presented strategy for power batteries at different temperatures could reach the goal of the overall error within 1% under CLTC conditions with well robustness and accuracy.

Keywords: lithium-ion battery; metabolic even grey model; parameter identification; state of charge estimation

Citation: Sun, Q.; Wang, S.; Gao, S.; Lv, H.; Liu, J.; Wang, L.; Du, J.; Wei, K. A State of Charge Estimation Approach for Lithium-Ion Batteries Based on the Optimized Metabolic EGM(1,1) Algorithm. *Batteries* **2022**, *8*, 260. <https://doi.org/10.3390/batteries8120260>

Academic Editors: Remus Teodorescu and Xin Sui

Received: 26 September 2022

Accepted: 25 November 2022

Published: 28 November 2022

Publisher's Note: MDPI stays neutral with regard to jurisdictional claims in published maps and institutional affiliations.



Copyright: © 2022 by the authors. Licensee MDPI, Basel, Switzerland. This article is an open access article distributed under the terms and conditions of the Creative Commons Attribution (CC BY) license (<https://creativecommons.org/licenses/by/4.0/>).

1. Introduction

The air pollution and energy shortages caused by automobile exhaust emissions have become increasingly prominent, along with the rapid development of the automobile industry. On account of high energy density, long life cycle, environmental protection, and pollution-free characteristics, lithium-ion batteries are becoming more and more important as power batteries for electric vehicles (EV) [1–5]. The attenuation of the battery during use is accompanied by changes in parameters such as capacity and impedance, which directly affect the reliability of battery operation. In order to ensure power, economy, and safety operation for EVs, battery state assessment is particularly important. Conventional battery state prediction methods mainly predict the battery state by detecting parameters such as battery charge and discharge rate, battery life, and open circuit voltage (OCV). Due to the complicated relationship between these parameters and the state of charge (SOC), traditional experimental methods have low prediction accuracy and low reliability [6–13]. Owing to the time-varying and non-linear characteristics of the battery system, the high-precision prediction of the battery state is undoubtedly an arduous task.

The significance of accurate battery modeling is that it could express the internal and external battery characteristics for different structures and different driving conditions,

which can be of much help in the optimal development of lithium-ion batteries. The equivalent circuit model (ECM) and electrochemical model (EM) approaches are widely employed to perform the characteristics of lithium-ion batteries for SOC estimation [14–18]. The EM describes the battery's dynamic characteristics based on differential iterations, which could be much more complicated. As a result, the EM method is usually adopted in battery design applications. In addition, current battery models rarely consider the effect of temperature on model parameters. With regard to the ECM with electrical components such as resistance and capacitor, this physical model is widely employed in battery management systems (BMS), since it could offer trade-off solutions with complexity and accuracy. Much research has shown the ECM is featured in SOC estimation, and the model is capable of exactly describing the physical and chemical characteristics of lithium-ion batteries, and satisfying the BMS requirement with low calculation cost [19–23]. Furthermore, the Extended Kalman Filter (EKF) algorithm depends on the battery state space model and employs a recursive iteration method to linearize the battery SOC [24,25]. Its accuracy is significantly influenced by the model's preciseness. Although the Unscented Kalman Filter (UKF) algorithm employs statistical linearization to reduce error and calculation, the SOC estimation accuracy still fluctuates along with the unit model [26–30]. Model-based methods could illustrate the physical and chemical characteristics of the battery, but the correctness of the parameters relies on the accuracy and robustness of the battery model [31–35]. In recent years, battery forecasting has developed towards non-modeling. The methods based on data-driven and statistical analysis mainly include the time sequence method, support vector machine method, and Markov method [36–39]. The sequential method can describe the periodic law of data changes, but it is unrealistic to record the data of various working conditions during the entire battery life cycle, and it is difficult to establish the learning model [40–43]. Although the support vector machine method has high accuracy, the amount of training data is large and time-consuming. The Markov method can reflect the periodic change characteristics of data and has strong randomness, but it is difficult to determine the situational state set.

Grey System Theory is widely used in various fields, and successfully solves the problem of incomplete information prediction. Grey Model-GM(1,1) is an approach that employs a small amount of incomplete data samples to establish a grey prediction model and then describes the development trend in a long-term predictive manner [44,45]. The advantages of rapid prediction have been widely accepted. With the extension of battery life, the parameters and performance of the battery also change correspondingly, and there're obvious uncertainties in estimating the SOC value with raw data. The traditional Even Grey Model-EGM(1,1) predicts that the cumulative error is relatively large and cannot reflect the periodic changes in the data [46–48]. The Metabolic Even Grey Model-MEGM(1,1) method is based on the latest data generated by the system and adopts the original data in the rolling deletion system to establish a new data sequence, thereby establishing a lithium-ion battery state estimation model, which can reflect the characteristics of the latest data in real time. Especially with the accumulation of system variables, when the battery system has parameter perturbation or sudden change, the algorithm based on MEGM(1,1) iterative model can achieve accurate SOC estimation of lithium battery.

In recent years, for the sake of lacking its own driving cycles, China directly cited the *new European driving cycle* (NEDC) driving standard, and it has significant influence in promoting the development of the automotive industry of China [49]. Nevertheless, along with the change in vehicle ownership, road structure and traffic condition in China, the endurance range of EVs under NEDC operating conditions has a large deviation from the actual driving situation in China. Furthermore, since the NEDC does not comply with the characteristics of the actual driving behavior of vehicles in China, it could not actually denote the real application effects of energy-saving and emission-reduction technologies, such as the idle start–stop and brake energy regeneration technology [50].

In addition, the *world-harmonized light-duty vehicle test cycle* (WLTC) was developed employing the actual driving behavior data collected through six regions, including Amer-

ica, Japan, India, Korea, the EU, and Switzerland. However, it is lacking Chinese data acquisition [49,51]. With different levels of congestion, WLTC driving condition better reflects the characteristics of fast and slow vehicle speeds, but the idling ratio and average speed of the two main operating conditions under WLTC condition are quite different from the actual operating conditions in China [51]. Thus, for China, the WLTC driving condition could not provide a suitable solution to solve the problem during the NEDC driving cycles mentioned previously. In order to comply with the real and much more critical driving conditions, the local test cycle *China Light-duty Vehicle Test Cycle* (CLTC) for endurance certification of EVs was announced by the *Ministry of Industry and Information Technology* (MIIT) of China.

For the modeling of the battery pack, the data-driven approach based on Gaussian process regression is proposed to put forward a feasible solution with non-linear approximation, nonparametric modeling, and probabilistic prediction [52]. As the battery pack includes hundreds of cells in series and parallel, inconsistencies among the cells will be difficult to build an accurate physical model for their behavior performance. As a result, the widely employed model-based approaches are unsuitable for SOC estimation of battery packs [53,54]. In the paper, for the sake of accurate SOC estimation of the lithium-ion battery cell, the characteristics of the battery with varied ambient temperatures are experimentally studied. The *Thevenin* equivalent circuit model with the sixth-order polynomial of OCV–SOC function relation is derived by exploiting the physical characteristics of the lithium-ion battery cell. Furthermore, along with the mechanism analysis of the traditional GM(1,1) approach is analyzed in detail, the optimized MEGM(1,1) algorithm is put forward based on the presented ECM. The estimation accuracy of the employed approach is explored via an experimental platform for the lithium-ion battery, which works under the CLTC driving condition with five different temperatures. All the experimental and theoretical results, compared with the traditional GM(1,1) estimation method, illustrate that the optimized MEGM(1,1)-based SOC estimation approach is with fast convergence, good robustness, and well accuracy for the critical driving condition.

2. Lithium-Ion Batteries' Modeling

There are various kinds of battery modeling methods, among which the *Thevenin* model for a battery has the characteristics of simple operation and it could illustrate the steady and transient characteristics of batteries. Therefore, this paper employs this modeling approach to establish the state space function of the battery. In addition, the *Thevenin* topology for lithium-ion battery is displayed in Figure 1, where V_{ocv} is the electromotive force of the battery, R_1 and R_2 are defined as ohmic internal resistor and polarization resistor, and C is the polarization capacitor, which is connected in parallel with the polarization resistance R_2 .

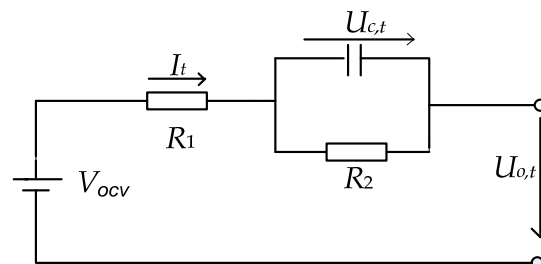


Figure 1. *Thevenin* topology for lithium-ion battery.

By means of the *Kirchhoff* and *Thevenin* principles, the expression for batteries' equivalent topology could be expressed in the following forms:

$$V_{ocv} = U_{o,t} + R_1 I_t + U_{c,t} \tag{1}$$

$$I_t = \frac{U_{c,t}}{R_2} + C \frac{dU_{c,t}}{dt} \tag{2}$$

The notation V_{ocv} denotes the battery's open circuit voltage, and OCV reflects the relationship function with respect to SOC as $V_{ocv} = F(S_t)$. $U_{o,t}$ is the terminal voltage of the battery, and $U_{c,t}$ is the polarization voltage. Thus, SOC could be derived through the current integration method.

$$S_t = S_{t_0} - \frac{1}{Q_0} \int_{t_0}^t \eta I_t dt \tag{3}$$

where η is the battery's discharge efficiency, Q_0 is battery capacity, and S_t is the SOC value of the battery at the moment t . The state space equation could be represented by means of integrating and discretizing the formulas consequently, as:

$$\left\{ \begin{aligned} \begin{bmatrix} S_{t+\Delta t} \\ U_{c,t+\Delta t} \end{bmatrix} &= \begin{bmatrix} 1 & 0 \\ 0 & \exp(-\frac{\Delta t}{R_2 C}) \end{bmatrix} \begin{bmatrix} S_t \\ U_{c,t} \end{bmatrix} + \begin{bmatrix} -\frac{\eta \Delta t}{Q_0} \\ R_2(1 - \exp(-\frac{\Delta t}{R_2 C})) \end{bmatrix} I_t + \begin{bmatrix} w_{1,t} \\ w_{2,t} \end{bmatrix} \\ U_{o,t} &= F(S_t) - R_1 I_t - U_{c,t} + v_t \end{aligned} \right. \tag{4}$$

where $x_t = [S_t, U_{c,t}]^T$ is defined as the state variable, $U_{o,t}$ is the observation variable, I_t is the control variable, $w_t = [w_{1,t}, w_{2,t}]^T$ is systematic noise, v_t is observation noise. Consequently, the coefficient matrix of the battery's state space model can be represented as:

$$\left\{ \begin{aligned} A_t &= \begin{bmatrix} 1 & 0 \\ 0 & \exp(-\frac{\Delta t}{R_2 C}) \end{bmatrix} \\ B_t &= \begin{bmatrix} -\frac{\eta \Delta t}{Q_0} \\ R_2(1 - \exp(-\frac{\Delta t}{R_2 C})) \end{bmatrix} \\ C_t &= [\frac{\partial F(S_t)}{\partial S_t} \Big|_{S_t=S_t^-}, -1] \end{aligned} \right. \tag{5}$$

The OCV of the battery is not completely equivalent to the electromotive force due to the hysteresis effect, but when the battery is fully left standing, the two values are very close, and it is difficult to directly measure the real electromotive force. Therefore, in actual research, the OCV of the battery is usually used to describe its electromotive force under the SOC value. The OCV–SOC correspondence is the key performance parameter of the battery. It is often employed to illustrate the working state of the battery and perform SOC calibration with the necessary parameters for establishing the battery model.

Before performing simulation and estimation for the battery's SOC, parameter identification is performed on the *Thevenin* equivalent circuit topology, and discharge test along with pulse power features is also conducted. The CB2P0 type cell of LiFePO₄ lithium-ion battery is employed for an experiment, and the specifications are displayed in Table 1.

Table 1. Specifications of CB2P0 lithium-ion battery.

Parameters	Values
Nominal Capacity (Ah)	30
Rated Voltage (V)	3.2
Charge Cutoff Voltage (V)	3.65
Discharge Cutoff Voltage (V)	2.5
Charge Temperature (°C)	0~55
Discharge Temperature (°C)	-25~55

The accurate SOC estimation for lithium-ion batteries' performance prediction and durability evaluation is of paramount importance, which is critical to ensure the reliability and stability of electric vehicles. The identification mechanism for the battery's parameters is mainly based on its physical behavior under different working temperatures. For the sake of accurate battery parameter identification, the pulse discharge test is conducted in this study during the range of $-25\text{ }^{\circ}\text{C}$ to $55\text{ }^{\circ}\text{C}$. According to the requirement of *ISO12405-2: 2012 for lithium-ion traction battery packs and system applications*, the battery is discharged at the current of $C/3$ to the cutoff voltage of 2.5V. The characteristics curve between the battery's SOC and OCV is illustrated in Figure 2.

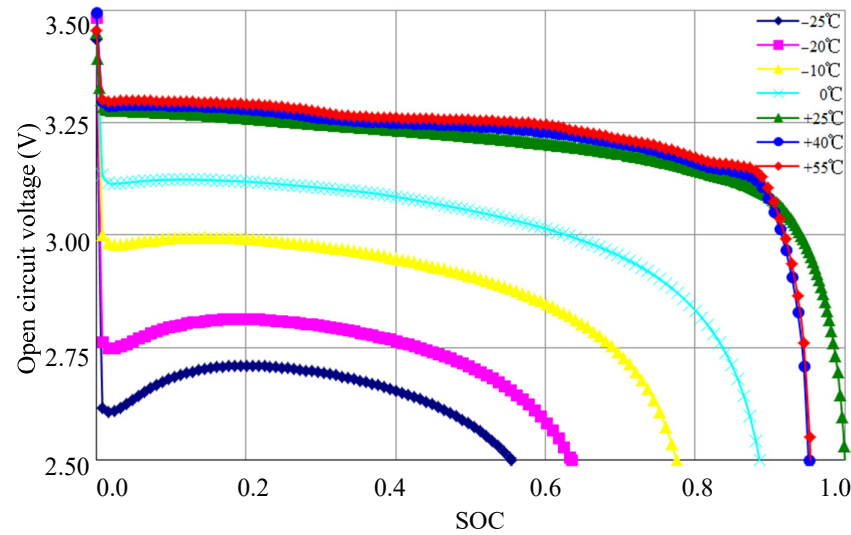


Figure 2. Characteristics curves on OCV and SOC.

As shown in Figure 2, under the condition of a small rate discharge, the discharge capacity can basically reach the rated value at room temperature. The performance of LiFePO_4 batteries at low temperatures will decrease significantly. At the same time, as the discharge rate increases, the impact of temperature on battery performance will become more and more obvious. The curve fitting method by means of *least squares* is employed to identify the non-linear functional relation between OCV and SOC.

For the sake of accurately fitting the experimental result of the lithium-ion battery, the sixth-order polynomial could be performed by means of the function:

$$V_{ocv}(SOC) = K_6 \cdot SOC^6 + K_5 \cdot SOC^5 + K_4 \cdot SOC^4 + K_3 \cdot SOC^3 + K_2 \cdot SOC^2 + K_1 \cdot SOC^1 + K_0 \tag{6}$$

where K_i ($i = 0, 1, 2, \dots$) is in reference to the specific ambient temperature, it influences the accuracy of the characteristic polynomial, which could be derived through the experimental pulse discharge results. The derived values of K_i under the various ambient temperatures are displayed in Table 2. Based on the sixth-order polynomial, a three-dimensional map of Temperature-SOC-OCV is illustrated in Figure 3 correspondingly.

Table 2. Coefficient values under different operating temperatures.

Coefficient	$-25\text{ }^{\circ}\text{C}$	$-20\text{ }^{\circ}\text{C}$	$-10\text{ }^{\circ}\text{C}$	$0\text{ }^{\circ}\text{C}$	$+25\text{ }^{\circ}\text{C}$	$+40\text{ }^{\circ}\text{C}$	$+55\text{ }^{\circ}\text{C}$
K_0	2.5802	2.7285	2.9621	3.0937	3.2595	3.2159	3.2143
K_1	1.2526	0.958	0.7823	0.9278	1.0965	2.8663	3.2648
K_2	-0.7987	-3.2591	-7.4156	-9.5828	-14.302	-30.61	-34.814
K_3	-25.623	4.133	35.141	43.355	65.984	133	151.43
K_4	99.131	-9.5266	-91.694	-99.723	-141.04	-277.11	-314.99
K_5	-146.39	24.44	116.65	109.91	140.22	273.9	310.24
K_6	73.74	-23.711	-57.662	-46.669	-52.579	-103.23	-116.37

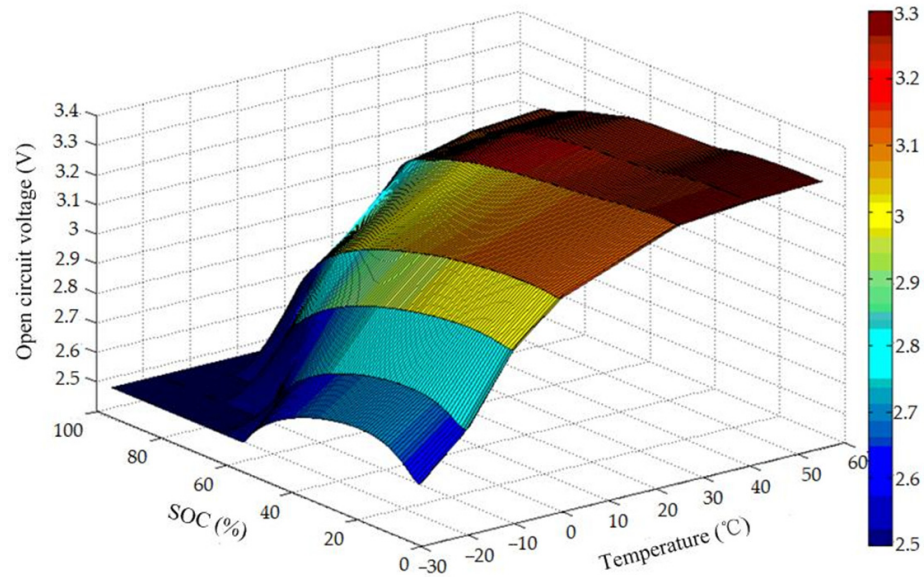


Figure 3. Three-dimensional map of Temperature-SOC-OCV.

The functional relation between OCV and SOC is non-linear, and parameter identification in the battery state space model could be achieved through the change characteristics of the terminal voltage during the pulse discharge experiment. At the ambient condition of 25 °C, the power battery is discharged along with the current of 1 C for 5 min, the discharge is stopped for 10 min, and then the battery is discharged for 5 min at the same current. A single pulse is selected to perform parameter identification on the battery model, and the dynamic curve of the battery’s terminal voltage is shown in Figure 4.

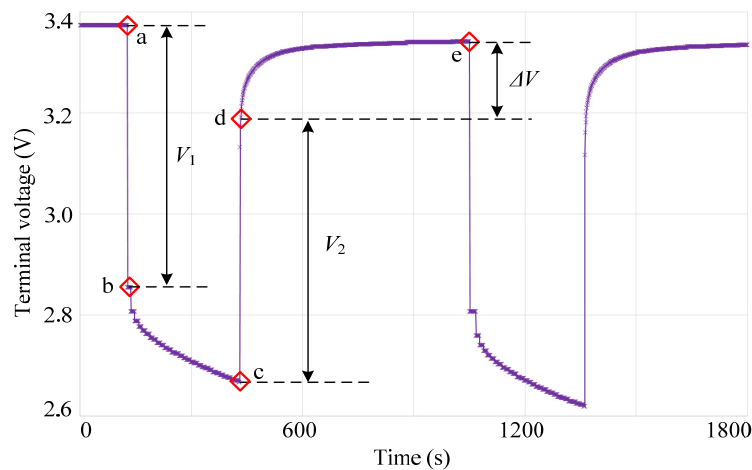


Figure 4. Terminal voltage of battery after discharging current pulse.

As to the *Thevenin* model shown in Figure 1, the terminal voltage changes corresponding to the discharging current pulse. Since the voltage of polarization capacitor C is not suddenly changed while starting discharging, the ohmic internal resistance R_1 and the polarization resistance R_2 are then identified according to the terminal voltage curve. Furthermore, regarding to the transient characteristics of RC topology, the battery’s terminal voltage increased to 86.5% ΔV needs twice constant Γ ($\Gamma = R_2 \times C$), which is identified with the terminal voltage curve. Consequently, the model parameters can be performed by means of the following form:

$$\begin{cases} R_1 = \frac{|V_T(t_a) - V_T(t_b)| + |V_T(t_d) - V_T(t_c)|}{2|I_{1C}|} \\ R_2 = \frac{|V_T(t_e) - V_T(t_d)|}{|I_{1C}|} \end{cases} \quad (7)$$

The dynamic battery parameter identification model based on temperature, voltage, and SOC is established by employing the least squares principle to fit the polarization effect parameters, and the established battery mathematical model could better adapt to the lithium battery performed with rich experimental waveforms. However, it can be seen that at different temperatures, the OCV-SOC curves are different, which indicates that the electrode characteristics of the battery are influenced by temperature, which will affect the SOC estimation. During the parameter identification process for the physical model of a fixed lithium-ion battery, the model parameters are consumed to be constant, which could affect the practicability of the presented estimation method for the sake of the variable temperatures. In order to further improve the estimation accuracy, the ongoing study will be towards the iterative learning-based on-line prediction approach that can precisely identify the parameters associated with the temperature and SOC.

3. Estimation Mechanism Based on Optimized MEGM(1,1)

3.1. General Principle of GM(1,1)

The traditional GM(1,1) is an approach that employs a small amount of incomplete data samples to establish a grey prediction model, and then describes the development trend in a long-term predictive period. GM(1,1) approach is to take the data sequence of lithium-ion batteries which changes with time as the original data sequence [44]. Through the cumulative calculation of the original data, a new data sequence is obtained. Furthermore, the relevant whitening differential equation is established with the solution derivation. Thereby, the grey estimation model for the lithium-ion battery state can be obtained, which could reflect the real-time features of a battery system. The derivation process of traditional GM(1,1) for SOC estimation is briefly described as follows [45].

(1) Extraction of battery history data: x_{SOC} , x_V , x_I and x_T . Where x_V , x_I and x_T are correlation factor series for input parameters, x_{SOC} is target SOC sequence for output parameters.

$$\begin{cases} x_V = (V_1, V_2, \dots, V_n) \\ x_I = (I_1, I_2, \dots, I_n) \\ x_T = (T_1, T_2, \dots, T_n) \\ x_{SOC} = (SOC_1, SOC_2, \dots, SOC_n) \end{cases} \quad (8)$$

(2) Perform 1st-order Accumulated Generating Operation (1-AGO) for the battery's data.

$$\begin{cases} x_V^1 = (V_1^1, V_2^1, \dots, V_n^1) \\ x_I^1 = (I_1^1, I_2^1, \dots, I_n^1) \\ x_T^1 = (T_1^1, T_2^1, \dots, T_n^1) \\ x_{SOC}^1 = (SOC_1^1, SOC_2^1, \dots, SOC_n^1) \end{cases} \quad (9)$$

(3) Generate the mean values of consecutive neighbor sequences.

$$\begin{cases} Z_V = (V_1, V_2, \dots, V_m) \\ Z_I = (I_1, I_2, \dots, I_m) \\ Z_T = (T_1, T_2, \dots, T_m) \\ Z_{SOC} = (SOC_1, SOC_2, \dots, SOC_m) \end{cases} \quad (10)$$

(4) Construct the whitening function for GM(1,1):

$$x_{SOC}(t_k) + a\Delta t_k Z_{SOC}(t_k - \tau) = b_2 x_V^1(t_k - \tau) t_k^\gamma \Delta t_k + b_3 x_I^1(t_k - \tau) t_k^\gamma \Delta t_k + b_4 x_T^1(t_k - \tau) t_k^\gamma \Delta t_k \quad (11)$$

where the time interval $\Delta t_k = t_k - t_{k-1}$, γ and τ are the iteration coefficients. In order to make the model as accurate as possible and to minimize the average relative error as the optimization objective of the whitening function, the constructed function related to parameters γ and τ is as:

$$f(\tau, \gamma) = \frac{1}{n-1} \sum_{i=2}^n \frac{x_{SOC}^1(i) - x_{SOC}(i)}{x_{SOC}(i)} \tag{12}$$

It could be seen this method could be easily utilized due to the advantage of rapid prediction. However the coefficients γ and τ are fixed for the conventional GM(1,1), it is unsuitable for massive data estimation. With the extension of battery life, the parameters and performance of the battery also change correspondingly, and there're obvious uncertainties in estimating the SOC value with raw data. The interference noise with external fluctuation and various driving conditions should be regarded during practical application. Thus the cumulative error is relatively large and cannot reflect the periodic changes in the data.

3.2. Principle of Optimized MEGM(1,1)

While the GM(1,1) model is employed for state evaluation of lithium-ion batteries, the closer the battery data is to the original time, the more accurate the prediction will be. Therefore, the modeling sequence should follow the change in the battery system by removing the oldest data sequence to reflect the updated characteristics. The MEGM(1,1) model is automatically updated and identified with each prediction, so the model has strong adaptability. After obtaining the closest information by the estimation, the original data sequence $x(0)$ is removed from this sequence, and the metabolic data sequence $x(m+1)$ is introduced as the original sequence to reconstruct MEGM(1,1) model [44,45,47]. Tracking the test data information as input, and using the current information to establish the prediction model until the accurate estimation target is reached, the input sequence and prediction sequence are updated iteratively, as shown in Figure 5.

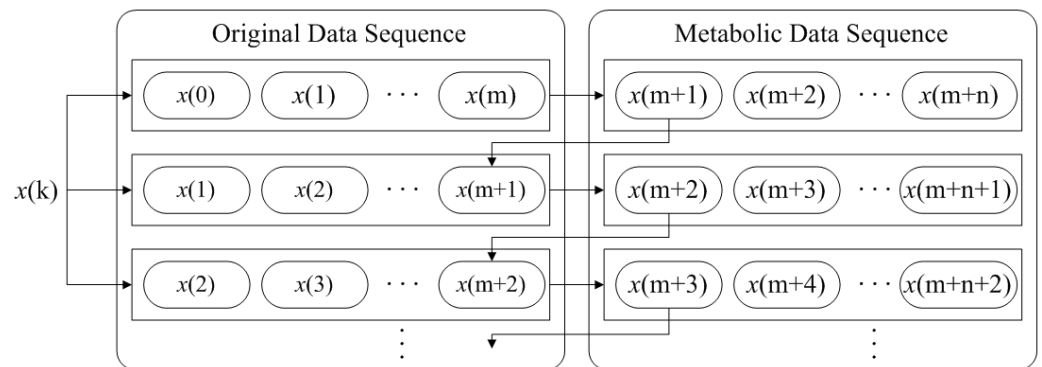


Figure 5. Diagram of rolling optimization strategy for MEGM(1,1).

In order to increase the accuracy of the extended data, the original data sequence is divided into q sub-sequences with different sample numbers.

$$\begin{cases} X_1 = \{x_1(0), x_1(1), \dots, x_1(r)\} \\ X_2 = \{x_2(1), x_2(2), \dots, x_2(r)\} \\ \dots \\ X_q = \{x_q(q-1), x_q(q-2), \dots, x_q(r)\} \end{cases} \tag{13}$$

where

$$x_\alpha(\beta) = x_{\alpha+1}(\beta)|_{\alpha=1,2,\dots,q;\beta=1,2,\dots,r} \tag{14}$$

The MEGM(1,1) dynamic equivalent topology could be represented through the first-order differential function including one single variable, which is fundamental for the grey estimation. Define the feature data sequence in the form:

$$X = \{x(0), x(1), \dots, x(r)\} \tag{15}$$

The data sequence generated by the means of the first-order accumulation is:

$$\begin{cases} x^{(1)}(m) = \sum_{i=1}^m x(i) \\ X^{(1)} = \{x^{(1)}(1), x^{(1)}(2), \dots, x^{(1)}(r)\} \end{cases} \tag{16}$$

where sequence $x^{(1)}$ is defined as 1-AGO. Furthermore, sequence $W^{(1)}$ is assumed as the information data produced through the average value of consecutive neighbors of $X^{(1)}$, given by:

$$\begin{cases} W^{(1)} = \{w^{(1)}(2), w^{(1)}(3), \dots, w^{(1)}(n)\} \\ w^{(1)}(\zeta) |_{\zeta=1,2,\dots,n-1} = \frac{1}{2} [x^{(1)}(\zeta + 1) + x^{(1)}(\zeta)] \end{cases} \tag{17}$$

Then the fundamental form of the MEGM(1,1) estimation model is established as [45]:

$$x(k) + \varepsilon x^{(1)}(k) = \vartheta \tag{18}$$

The whitening differential equation for $X^{(1)}$ is performed as:

$$\frac{dx^{(1)}}{dt} + \varepsilon \cdot x^{(1)} = \vartheta \tag{19}$$

where ε is the development coefficient, ϑ is grey input. The following discretized expression can be derived:

$$\begin{cases} dx^{(1)} = x^{(1)}(\zeta + 1) - x^{(1)}(\zeta) \\ dt = \zeta + 1 - \zeta = 1 \end{cases} \tag{20}$$

Define the equation $x^{(1)}(\zeta) = \frac{1}{2}(x^{(1)}(\zeta + 1) + x^{(1)}(\zeta))$, hence Equation (19) could be expressed as follows:

$$x(\zeta + 1) = \varepsilon \left(-\frac{1}{2} (x^{(1)}(\zeta + 1) + x^{(1)}(\zeta)) \right) + \vartheta \tag{21}$$

In order to derive the solving solutions of parameters ε and ϑ , Equation (21) can be transformed as:

$$\begin{bmatrix} x(2) \\ x(3) \\ \dots \\ x(l) \end{bmatrix} = \varepsilon \begin{bmatrix} -\frac{1}{2} (x^{(1)}(1) + x^{(1)}(2)) \\ -\frac{1}{2} (x^{(1)}(2) + x^{(1)}(3)) \\ \dots \\ -\frac{1}{2} (x^{(1)}(l-1) + x^{(1)}(l)) \end{bmatrix} + \vartheta \begin{bmatrix} 1 \\ 1 \\ \dots \\ 1 \end{bmatrix} \tag{22}$$

In addition, according to Equation (22), the following equations are defined as:

$$\begin{cases} Y_r = [x(2) & x(3) & \dots & x(r)]^T \\ W^{(1)} = \begin{bmatrix} -\frac{1}{2}(x^{(1)}(1) + x^{(1)}(2)) \\ -\frac{1}{2}(x^{(1)}(2) + x^{(1)}(3)) \\ \vdots \\ -\frac{1}{2}(x^{(1)}(r-1) + x^{(1)}(r)) \end{bmatrix} \\ V = [1 \quad 1 \quad \dots \quad 1]^T \end{cases} \tag{23}$$

Based on the *least squares* estimation algorithm, the parameter matrix for MEGM(1,1) model could be performed by the form [55]:

$$\hat{a} = [\varepsilon \quad \vartheta]^T = \left([W^{(1)} \quad V][W^{(1)} \quad V]^T \right)^{-1} [W^{(1)} \quad V]^T Y_r \tag{24}$$

Thereby, the following expression can be written to compute solutions of parameters ε and ϑ , considering Equations (23) and (24), as:

$$Y_r = \varepsilon W^{(1)} + \vartheta V = [W^{(1)} \quad V] \begin{bmatrix} \varepsilon \\ \vartheta \end{bmatrix} \tag{25}$$

Define $x^{(1)}(1) = x(1)$, the solution of the whitening differential equation can be calculated as follows:

$$\hat{x}^{(1)}(\zeta + 1) = \left[x(1) - \frac{\vartheta}{\varepsilon} \right] e^{-\varepsilon\zeta} + \frac{\vartheta}{\varepsilon} \tag{26}$$

In order to extend the original data sequence of the lithium-ion battery, the restore sequence is derived by reductive generation, as:

$$\begin{aligned} x(\zeta + 1)|_{\zeta=r+1,r+2,\dots} &= \hat{x}^{(1)}(\zeta + 1) - \hat{x}^{(1)}(\zeta) \\ &= (1 - e^{-\varepsilon}) \left[x(1) - \frac{\vartheta}{\varepsilon} \right] e^{-\varepsilon\zeta} \end{aligned} \tag{27}$$

According to Equation (27), the fitting calculation of q sub-sequences in Equation (15) is carried out, and the result of fitting calculation $\hat{X}_i|_{i=1,2,\dots,q}$ is:

$$\begin{cases} \hat{X}_1 = \{\hat{x}_1(0), \hat{x}_1(1), \dots, \hat{x}_1(r), \hat{x}_1(r+1)\} \\ \hat{X}_2 = \{\hat{x}_2(1), \hat{x}_2(2), \dots, \hat{x}_2(r), \hat{x}_2(r+1)\} \\ \dots \\ \hat{X}_q = \{\hat{x}_q(q-1), \hat{x}_q(q-2), \dots, \hat{x}_q(r), \hat{x}_q(r+1)\} \end{cases} \tag{28}$$

The Grey Relation Function (GRF) $Y(X_\alpha, \hat{X}_\beta)$ is derived by calculating the original sequence and metabolic fitting sequence, as:

$$\begin{cases} Y(X_\alpha, \hat{X}_\alpha) = \frac{1}{r-\alpha} \sum_{\beta=\alpha}^r Y_\alpha(x_\alpha(\beta), \hat{x}_\alpha(\beta)) \\ Y_\alpha(x_\alpha(\beta), \hat{x}_\alpha(\beta)) = \frac{MIN+\rho MAX}{|x_\alpha(\beta) - \hat{x}_\alpha(\beta)| + \rho MAX} \\ MIN = \min|x_\alpha(\beta) - \hat{x}_\alpha(\beta)| \\ MAX = \max|x_\alpha(\beta) - \hat{x}_\alpha(\beta)| \end{cases} \tag{29}$$

As a result, the whitening equation with $-N - 1$ input parameters and one output parameter is established as follows [47]:

$$\frac{dX_1^{(1)}}{dt} + a_0 X_1^{(1)} = b_1 X_2^{(1)} + b_2 X_3^{(1)} + \dots + b_{N-1} X_N^{(1)} \tag{30}$$

where $a_0, b_1, b_2, \dots, b_{N-1}$ are function coefficients, $X_1^{(1)}$ is the output parameter, $X_2^{(1)}, X_3^{(1)}, \dots, X_{N-1}^{(1)}$ are the input parameters. Furthermore, the parameters are with strong coupling. Accordingly, the estimation result of the output parameter could be expressed as:

$$\begin{aligned} X_1^{(1)}(t) = & \left(X_1^{(1)}(1) - \frac{b_1}{a_0} X_2^{(1)}(t) - \frac{b_2}{a_0} X_3^{(1)}(t) - \dots - \frac{b_{N-1}}{a_0} X_N^{(1)}(t) \right) e^{-a_0 t} + \\ & \frac{b_1}{a_0} X_2^{(1)}(t) + \frac{b_2}{a_0} X_3^{(1)}(t) + \dots + \frac{b_{N-1}}{a_0} X_N^{(1)}(t) \end{aligned} \tag{31}$$

In this research, parameters x_V, x_I and x_T are input data sequence, x_{SOC} is SOC sequence for output parameters. So the expression can be transformed as:

$$\begin{aligned} X_{SOC}^{(1)}(t) = & \left(X_{SOC}^{(1)}(1) - \frac{b_1}{a_0} X_V^{(1)}(t) - \frac{b_2}{a_0} X_I^{(1)}(t) - \frac{b_3}{a_0} X_T^{(1)}(t) \right) e^{-a_0 t} + \\ & \frac{b_1}{a_0} X_V^{(1)}(t) + \frac{b_2}{a_0} X_I^{(1)}(t) + \frac{b_3}{a_0} X_T^{(1)}(t) \end{aligned} \tag{32}$$

Define:

$$D = \frac{b_1}{a_0} X_V^{(1)}(t) + \frac{b_2}{a_0} X_I^{(1)}(t) + \frac{b_3}{a_0} X_T^{(1)}(t) \tag{33}$$

Correspondingly, the SOC estimation value for lithium-ion batteries could be derived by means of the following equation.

$$\begin{aligned} X_{SOC}^{(1)}(t) = & \left\{ \left[X_{SOC}^{(1)}(1) - D \right] - X_{SOC}^{(1)}(1) \cdot \frac{1}{1+e^{-a_0 t}} + \right. \\ & \left. 2D \cdot \frac{1}{1+e^{-a_0 t}} \right\} \cdot (1 + e^{-a_0 t}) \end{aligned} \tag{34}$$

On the basis of the original data of lithium-ion batteries, the initial mathematical model and parameter identification are established. Furthermore, the Grey Relation Analysis (GRA) is introduced to figure out the new data by employing the original data, and then a new model is established instead of the original data. With the continuous use of metabolic update-data modeling, the state estimation of lithium-ion batteries is accurately established. Aiming at the requirements of SOC estimation and the non-linear characteristics of the dynamic battery system, an optimized MEGM(1,1) model is proposed to expand battery state data and introduce temperature factors into the prediction process to make SOC estimation much more accurate.

4. Experimental Verification and Analysis

In order to verify the effectiveness and accuracy of the presented estimation algorithm, an experimental platform for the battery system is established. The block diagram of the battery system’s test bench includes a High-Low temperature incubator (LJGDP-20R-E, LIK Industry Co., Ltd., Dongguan, China), a heavy-duty dual channel cycling station (AV-900, AeroVironment Inc., Simi Valley, CA, USA), a set of the measurement tool and control software, such as CANoe (VN1630A, Vector Co., Ltd., Stuttgart, Germany) and Labview, and a computer, as shown in Figure 6.

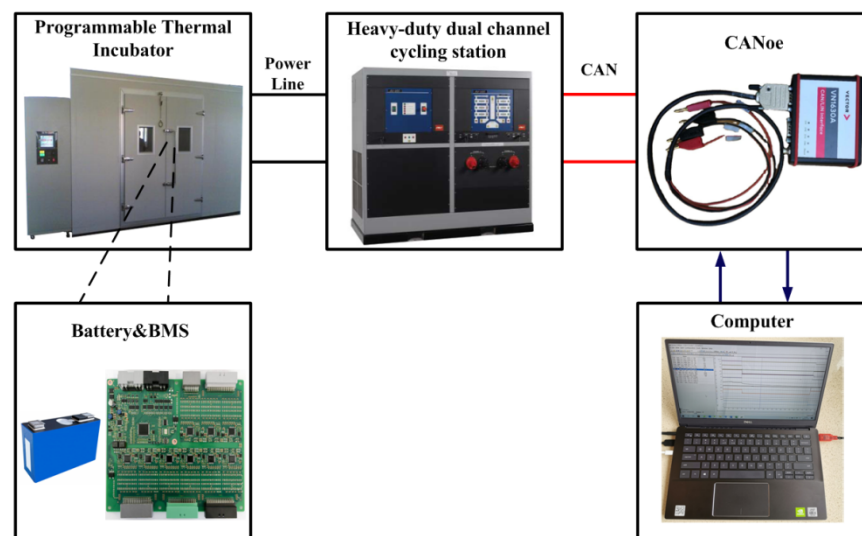


Figure 6. Block diagram of battery system test bench.

Under the CLTC driving condition, there is both driving discharge and regenerative charge, which fully considers the complexity of the road situations. For the single static charging of Li-ion battery, the charging station usually adopts constant current for charge and the SOC estimation is much more simplified. With regard to this research, we mainly discuss the SOC estimation performance of CB2P0 LiFePO₄ lithium-ion battery cells under CLTC driving conditions. This study focuses on characterizing the battery in dynamic real-time operation during vehicle CLTC driving conditions to optimize EV drivelines and accurate state estimation for EV manufacturers. In the experimental research, the battery cell is placed in an LJGDP-20R-E High-Low temperature incubator and stands for 16 h to achieve thermal balance. The AV-900 cycling station is utilized to simulate the demanded power sequence of CLTC working conditions, the driving cycles are performed, and one cycle period is 1800 s with a total of 36,000 s until the discharge cutoff voltage is achieved. In this research, the time interval of 10 Hz is employed for the battery system's data acquisition.

In the battery experiment system, the adopted CB2P0 cells are from the same batch with good consistency, so that random lithium cell is selected for experimental analysis, and the feasibility and effectiveness of the analysis principle are validated through numerical calculation and measurement results. Verification results under the CLTC driving condition at various temperature conditions of $-10\text{ }^{\circ}\text{C}$, $0\text{ }^{\circ}\text{C}$, $15\text{ }^{\circ}\text{C}$, $25\text{ }^{\circ}\text{C}$, and $35\text{ }^{\circ}\text{C}$ are obtained with estimation curves of the GM(1,1) and the optimized MEGM(1,1) approach, respectively. Furthermore, the enlarged view of discharging terminal voltage in one cycle for the time range of 16.8 ks–18.6 ks is also displayed in the following figures.

Figure 7 is the comparison results among the experimentally measured voltage, GM(1,1), and MEGM(1,1) estimation voltage with the enlarged view of discharging terminal cell voltage in one cycle for the time range of 16.8 ks–18.6 ks at the different ambient temperatures. On the basis of the measured big data, the battery's electrical characteristics are temperature-dependent with a three-dimensional map of Temperature-SOC-OCV, as the estimation of the terminal voltage performs much more accurately at $25\text{ }^{\circ}\text{C}$ and $35\text{ }^{\circ}\text{C}$, compared with the performance at $-10\text{ }^{\circ}\text{C}$, $0\text{ }^{\circ}\text{C}$ and $10\text{ }^{\circ}\text{C}$ under the CLTC driving condition. This is mainly because the conductivity of the electrolyte varies at different temperatures, and the migration speed of the lithium ions fluctuates with hysteretic characteristics regarding the OCV-SOC relation, which leads to the accumulation error for the model's parameter estimation. It can be seen that the estimated errors of terminal voltage are within 15 mV with rapid convergence characteristics.

Additionally, the initial SOC value would affect the convergence performance and the estimation accuracy. In order to demonstrate the performance of the proposed SOC

estimation approach and the characteristics of convergence, the initial SOC value is set to be 60% in the dynamic experiment. Figure 8 is the SOC comparison among the experimentally measured data, GM(1,1) and MEGM(1,1) estimation values with the enlarged view in one cycle for the time range of 16.8 ks–18.6 ks at the different ambient temperatures. In the research, the quantitative analysis approaches for SOC error evaluation after convergence are Root Mean Square Error (RMSE) and Mean Absolute Error (MAE), as are employed to illustrate the performance of the proposed SOC prediction model shown in Table 3. As can be displayed from the experimental results, regardless of the difference between the initial value and the real value of SOC, as the number of iterations increases, the SOC estimation value approximates the real value rapidly and the steady state error is within 1.00% after convergence by the optimized MEGM(1,1).

Table 3. Estimation analysis for GM(1,1) and MEGM(1,1) after convergence under CLTC.

Temperature	Model	RMSE	MAE
−10 °C	GM(1,1)	0.0175	0.0142
	MEGM(1,1)	0.0099	0.0079
0 °C	GM(1,1)	0.0174	0.0140
	MEGM(1,1)	0.0089	0.0061
+15 °C	GM(1,1)	0.0163	0.0129
	MEGM(1,1)	0.0072	0.0051
+25 °C	GM(1,1)	0.0144	0.0115
	MEGM(1,1)	0.0059	0.0046
+35 °C	GM(1,1)	0.0157	0.0122
	MEGM(1,1)	0.0069	0.0048

Generally, the optimized algorithm presents well robustness against initial SOC deviation and temperature variation, and the initial SOC value only affects the time taken for the SOC estimate to approach the real value, which does not affect the accuracy of the steady state SOC estimation even if the initial SOC has a large deviation. The close agreement between simulation results and experimental data on Li-ion batteries indicates that the presented MEGM(1,1) approach is capable of real-time updating battery model parameters, restraining system variation via self-adaption, and achieving accurate SOC prediction with less estimation error under the critical CLTC driving condition at the various ambient temperatures.

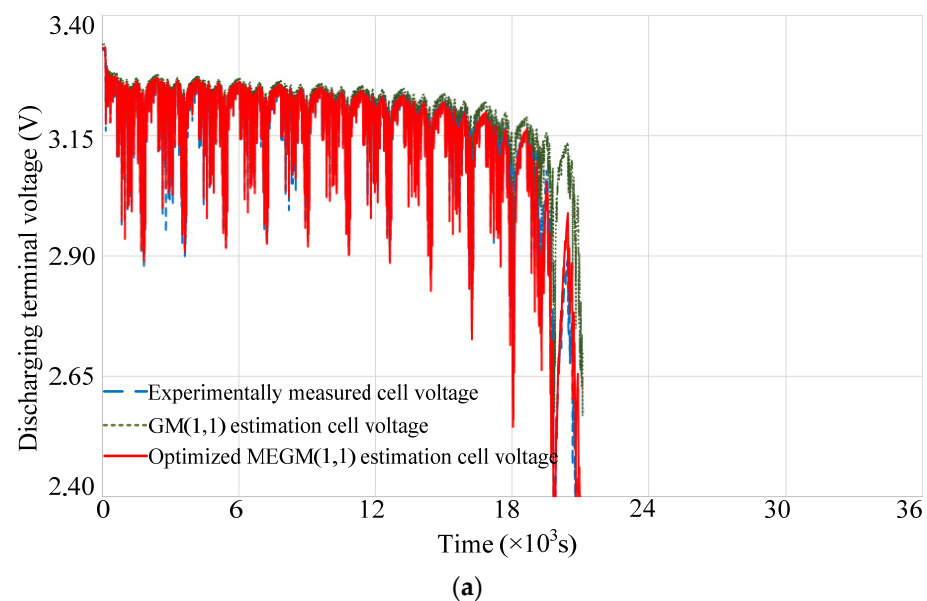
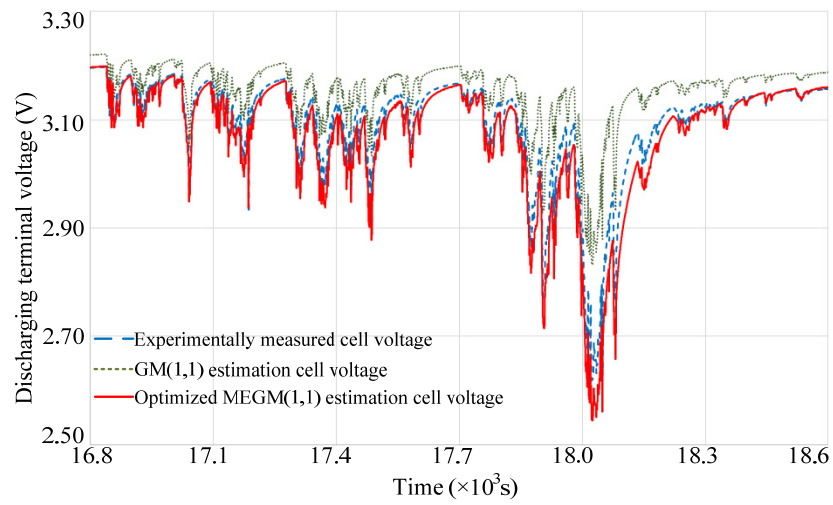
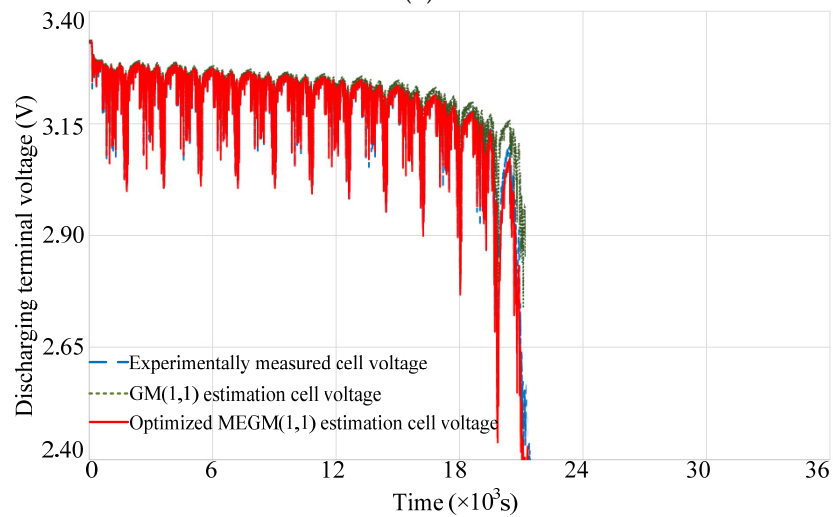


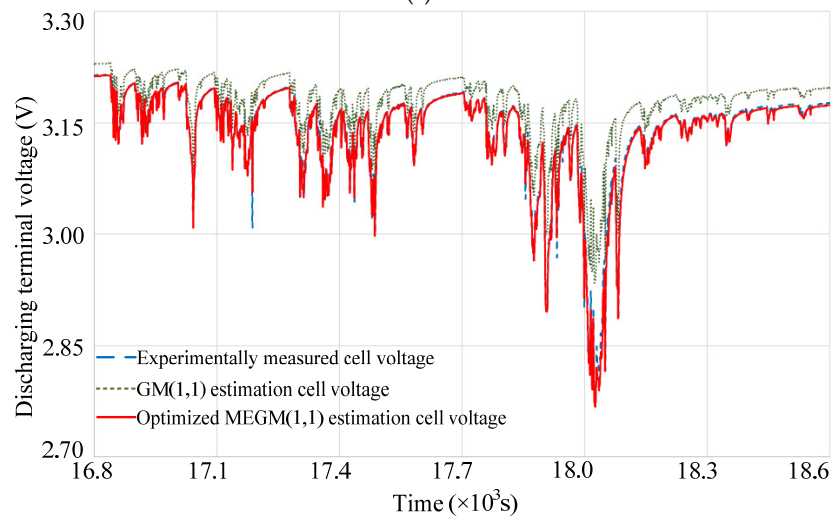
Figure 7. Cont.



(b)

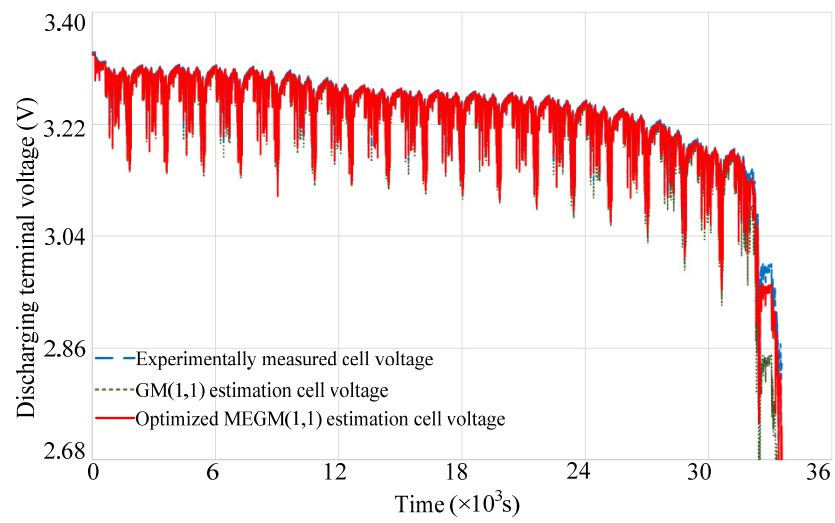


(c)

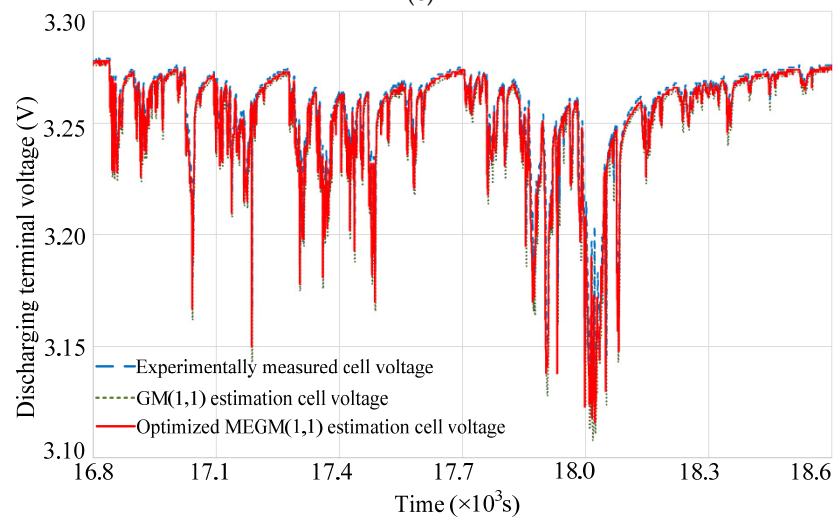


(d)

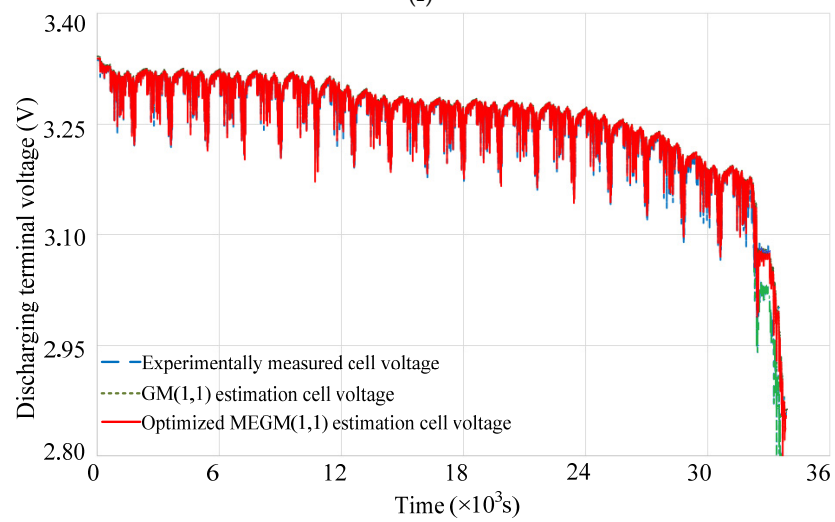
Figure 7. Cont.



(e)



(f)



(g)

Figure 7. Cont.

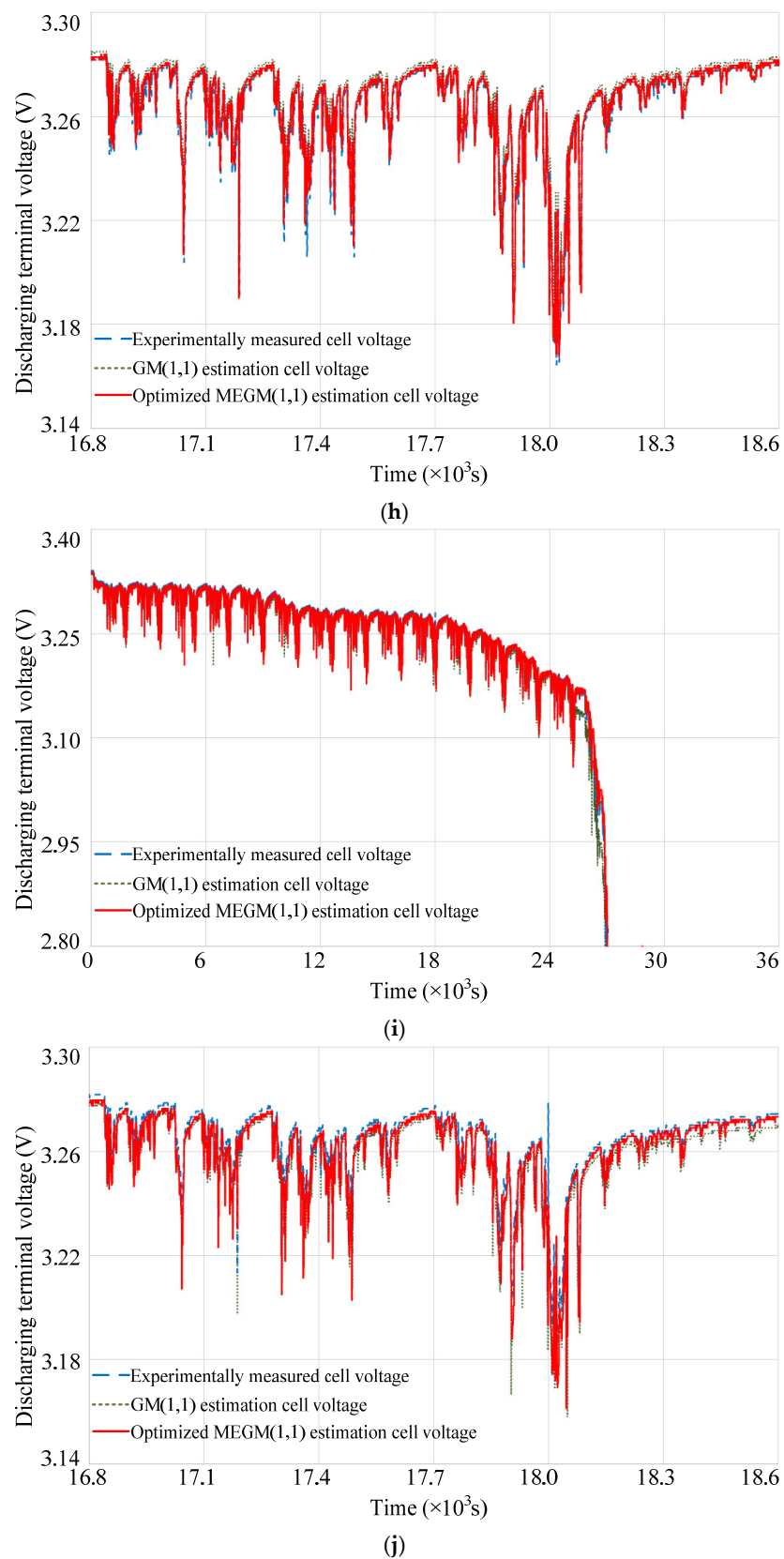
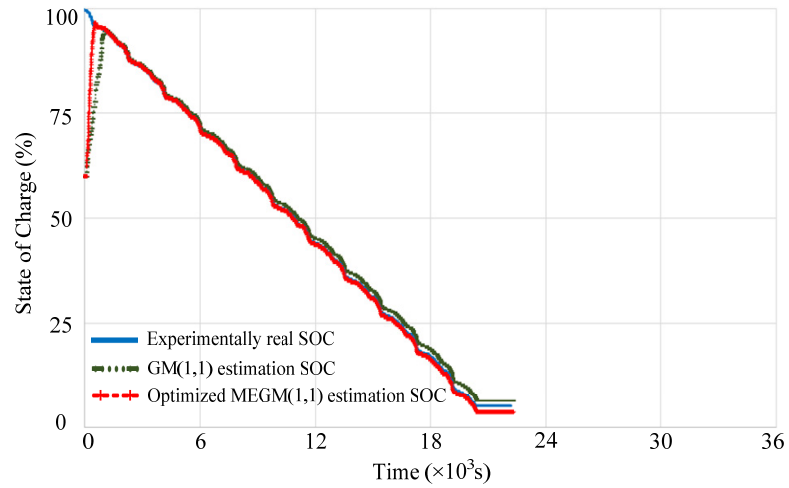
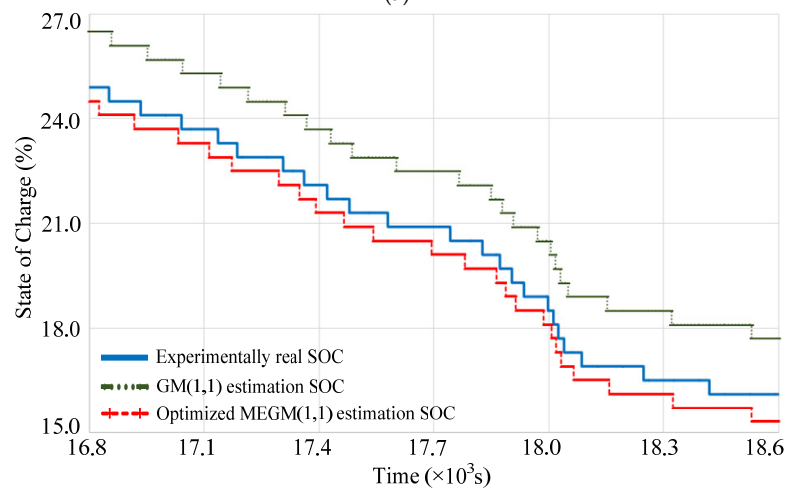


Figure 7. Verification results under the CLTC driving condition at the various temperatures: (a) voltage comparison among the measured data, GM(1,1) and MEGM(1,1) estimation at -10°C ; (b) the enlarged view of discharging terminal voltage in one cycle for the time range of 16.8 ks–18.6 ks

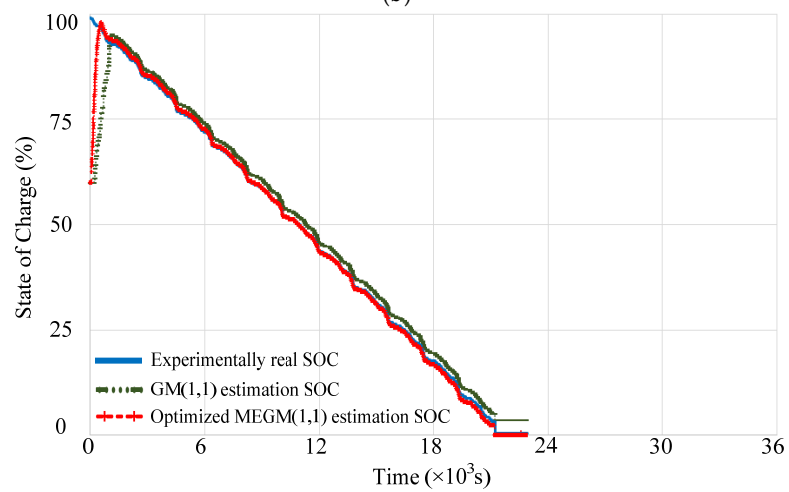
at $-10\text{ }^{\circ}\text{C}$; (c) voltage comparison at $0\text{ }^{\circ}\text{C}$; (d) the enlarged view at $0\text{ }^{\circ}\text{C}$; (e) voltage comparison at $15\text{ }^{\circ}\text{C}$; (f) the enlarged view at $15\text{ }^{\circ}\text{C}$; (g) voltage comparison at $25\text{ }^{\circ}\text{C}$; (h) the enlarged view at $25\text{ }^{\circ}\text{C}$; (i) voltage comparison at $35\text{ }^{\circ}\text{C}$; (j) the enlarged view at $35\text{ }^{\circ}\text{C}$.



(a)



(b)



(c)

Figure 8. Cont.

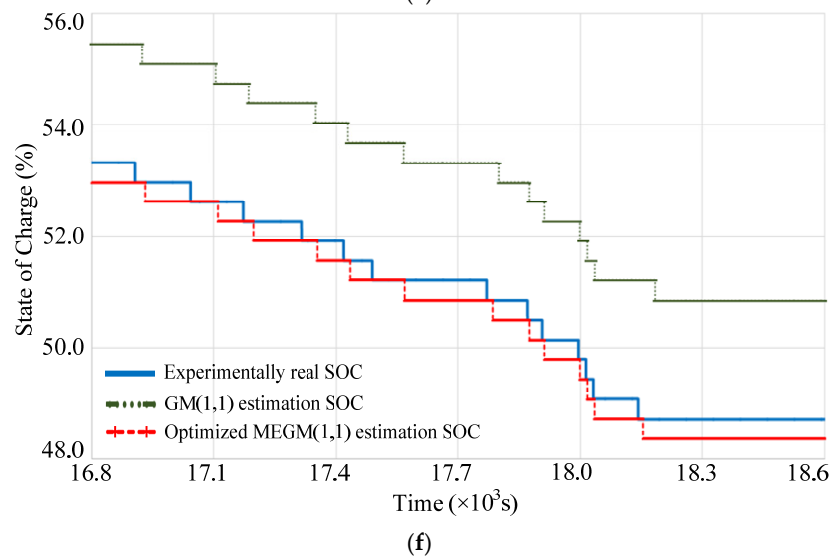
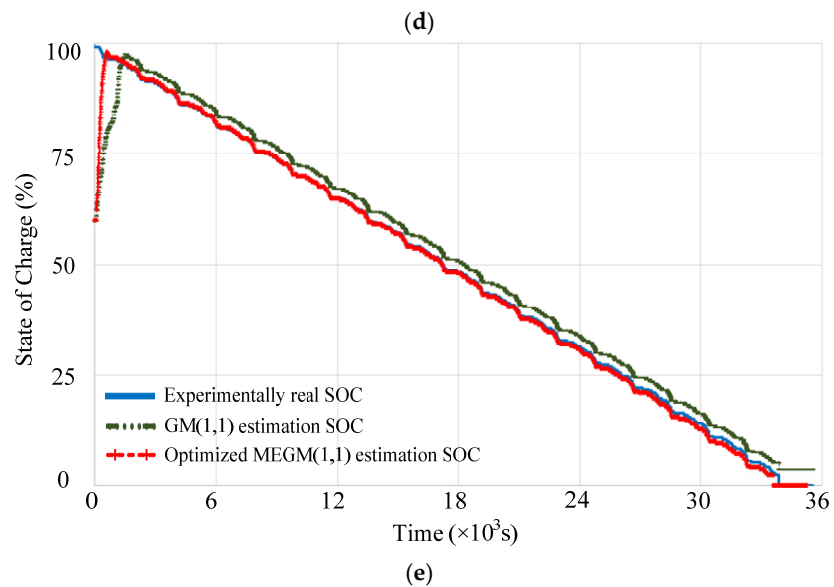
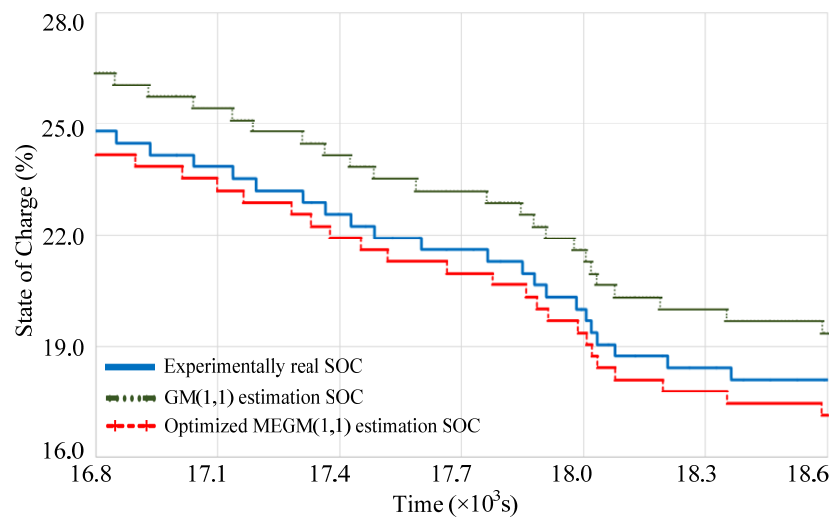


Figure 8. Cont.

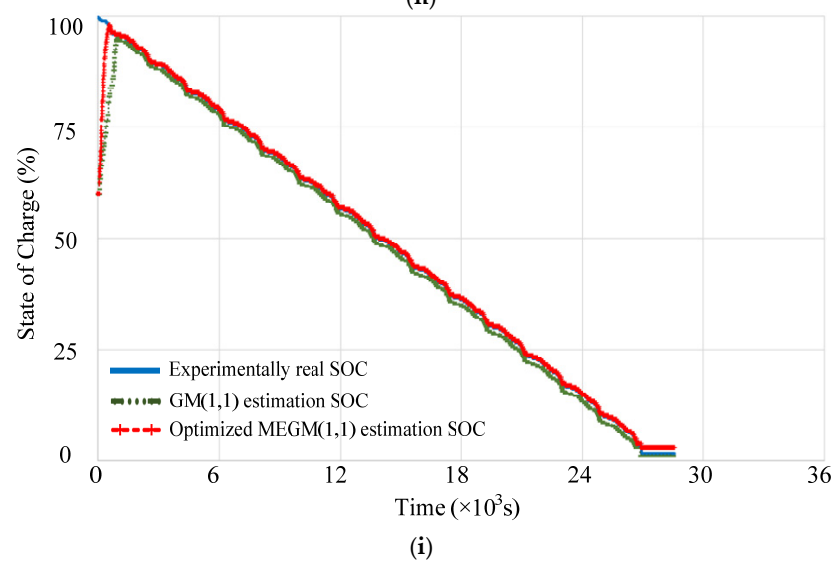
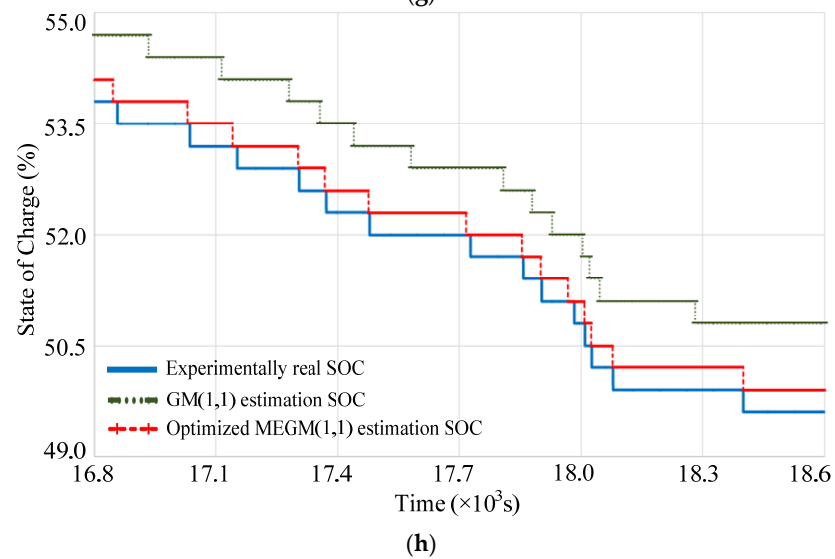
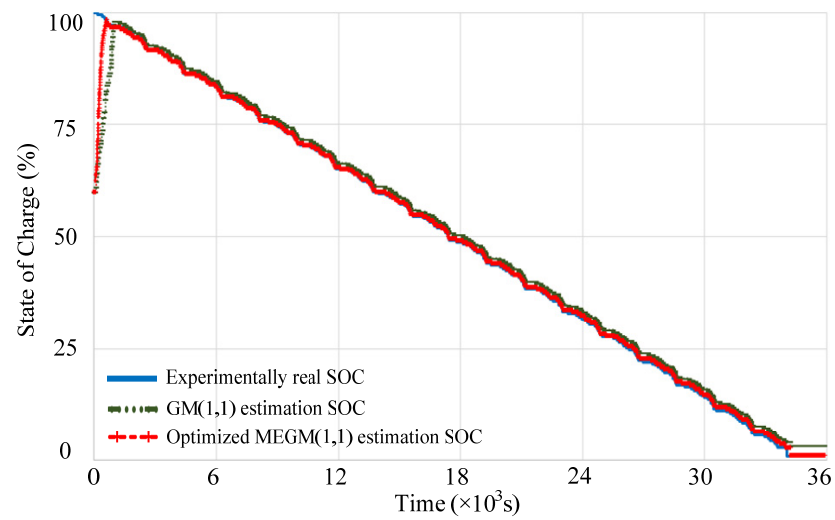


Figure 8. Cont.

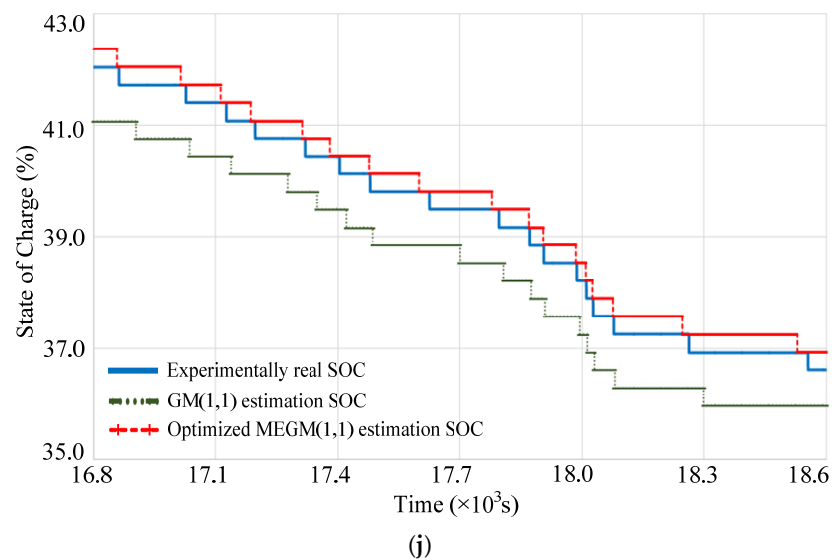


Figure 8. Verification results under the CLTC driving condition with initial SOC errors at the various temperatures: (a) SOC comparison among the experimental data, GM(1,1) and MEGM(1,1) estimation at $-10\text{ }^{\circ}\text{C}$; (b) the enlarged view of SOC in one cycle for the time range of 16.8 ks–18.6 ks at $-10\text{ }^{\circ}\text{C}$; (c) SOC comparison at $0\text{ }^{\circ}\text{C}$; (d) the enlarged view at $0\text{ }^{\circ}\text{C}$; (e) SOC comparison at $15\text{ }^{\circ}\text{C}$; (f) the enlarged view at $15\text{ }^{\circ}\text{C}$; (g) SOC comparison at $25\text{ }^{\circ}\text{C}$; (h) the enlarged view at $25\text{ }^{\circ}\text{C}$; (i) SOC comparison at $35\text{ }^{\circ}\text{C}$; (j) the enlarged view at $35\text{ }^{\circ}\text{C}$.

5. Conclusions

Through the statistical analysis of the experimental data obtained by charging and discharging stations and temperature control boxes to carry out battery test experiments at different temperatures, the battery capacity, ohmic resistance, and open circuit voltage for the parameter model are calibrated. The dynamic battery parameter identification model based on temperature, voltage, and SOC is established by employing the least squares principle to fit the polarization effect parameters, and the established battery mathematical model can better adapt to the lithium battery under the experiment. Aiming at the requirements of battery SOC estimation and the non-linear characteristics of dynamic battery systems, an optimized MEGM(1,1) model is proposed to expand battery state data and introduce temperature factors in the estimation process to make SOC estimation more accurate. The simulation results show that, compared with the traditional GM(1,1) algorithm, the SOC estimation based on the MEGM(1,1) strategy converges faster and the overall error is reduced. Therefore, the proposed optimization algorithm can make the estimated value meet the requirements of fast convergence and small error, which presents well robustness against initial SOC deviation and temperature variation. Experimental results also illustrate that the SOC estimation based on the proposed strategy for power lithium batteries at different temperatures could achieve the goal of an overall error within 1% under CLTC conditions with well robustness and accuracy.

Author Contributions: Conceptualization, Q.S. and S.W.; methodology, Q.S. and H.L.; software, S.W. and S.G.; validation, Q.S., S.W. and J.D.; formal analysis, K.W. and J.L.; investigation, S.G. and L.W.; resources, J.D. and L.W.; data curation, Q.S., S.W. and J.L.; writing—original draft preparation, Q.S.; writing—review and editing, Q.S. and H.L.; supervision, Q.S.; project administration, Q.S. and J.L.; funding acquisition, Q.S. and S.G. All authors have read and agreed to the published version of the manuscript.

Funding: This research was funded by the Scientific Research Project of Tianjin Municipal Education Commission, grant number 2020KJ093; and in the part by the National Key Research and Development Project of China, grant number 2018YFB0106102.

Data Availability Statement: Not applicable.

Conflicts of Interest: The authors declare no conflict of interest.

References

1. Kurzweil, P.; Frenzel, B.; Scheuerpflug, W. A Novel Evaluation Criterion for the Rapid Estimation of the Overcharge and Deep Discharge of Lithium-Ion Batteries Using Differential Capacity. *Batteries* **2022**, *8*, 86. [[CrossRef](#)]
2. Li, A.; Yuen, A.C.Y.; Wang, W.; Chen, T.B.Y.; Lai, C.S.; Yang, W.; Wu, W.; Chan, Q.N.; Kook, S.; Yeoh, G.H. Integration of Computational Fluid Dynamics and Artificial Neural Network for Optimization Design of Battery Thermal Management System. *Batteries* **2022**, *8*, 69. [[CrossRef](#)]
3. Dubarry, M.; Beck, D. Analysis of Synthetic Voltage vs. Capacity Datasets for Big Data Li-ion Diagnosis and Prognosis. *Energies* **2021**, *14*, 2371. [[CrossRef](#)]
4. Zhang, S.; Guo, X.; Dou, X.; Zhang, X. A rapid online calculation method for state of health of lithium-ion battery based on coulomb counting method and differential voltage analysis. *J. Power Sources* **2020**, *479*, 228740. [[CrossRef](#)]
5. Solaymani, S. CO₂ emissions patterns in 7 top carbon emitter economies: The case of transport sector. *Energy* **2019**, *168*, 989–1001. [[CrossRef](#)]
6. Theiler, M.; Schneider, D.; Endisch, C. Kalman Filter Tuning Using Multi-Objective Genetic Algorithm for State and Parameter Estimation of Lithium-Ion Cells. *Batteries* **2022**, *8*, 104. [[CrossRef](#)]
7. Sun, Q.; Lv, H.; Wang, S.; Gao, S.; Wei, K. Optimized state of charge estimation of lithium-ion battery in smes/battery hybrid energy storage system for electric vehicles. *IEEE Trans. Appl. Supercond.* **2021**, *31*, 3091119. [[CrossRef](#)]
8. Lv, J.; Jiang, B.; Wang, X.; Liu, Y.; Fu, Y. Estimation of the State of Charge of Lithium Batteries Based on Adaptive Unscented Kalman Filter Algorithm. *Electronics* **2020**, *9*, 1425. [[CrossRef](#)]
9. Xu, Y.; Hu, M.; Fu, C.; Cao, K.; Su, Z.; Yang, Z. State of Charge Estimation for Lithium-Ion Batteries Based on Temperature-Dependent Second-Order RC Model. *Electronics* **2019**, *8*, 1012. [[CrossRef](#)]
10. Hu, M.; Li, Y.; Li, S.; Fu, C.; Qin, D.; Li, Z. Lithium-ion battery modeling and parameter identification based on fractional theory. *Energy* **2018**, *165*, 153–163. [[CrossRef](#)]
11. Li, X.; Yuan, C.; Wang, Z. State of health estimation for Li-ion battery via partial incremental capacity analysis based on support vector regression. *Energy* **2020**, *203*, 117852. [[CrossRef](#)]
12. Huang, B.; Hu, M.; Chen, L.; Jin, G.; Liao, S.; Fu, C.; Wang, D.; Cao, K. A Novel Electro-Thermal Model of Lithium-Ion Batteries Using Power as the Input. *Electronics* **2021**, *10*, 2753. [[CrossRef](#)]
13. Hossain Lipu, M.S.; Hannan, M.A.; Hussain, A.; Ayob, A.; Saad, M.H.M.; Muttaqi, K.M. State of Charge Estimation in Lithium-Ion Batteries: A Neural Network Optimization Approach. *Electronics* **2020**, *9*, 1546. [[CrossRef](#)]
14. Li, X.; Huang, Z.; Tian, J.; Tian, Y. State-of-charge estimation tolerant of battery aging based on a physics-based model and an adaptive cubature Kalman filter. *Energy* **2021**, *220*, 119767. [[CrossRef](#)]
15. Ye, M.; Guo, H.; Cao, B. A model-based adaptive state of charge estimator for a lithium-ion battery using an improved adaptive particle filter. *Appl. Energy* **2017**, *190*, 740–748. [[CrossRef](#)]
16. Lian, B.; Sims, A.; Yu, D.; Wang, C.; Dunn, R.W. Optimizing LiFePO₄ battery energy storage systems for frequency response in the UK system. *IEEE Trans. Sustain. Energy* **2016**, *8*, 385–394. [[CrossRef](#)]
17. Jiang, K.; Gu, P.; Huang, P.; Zhang, Y.; Duan, B.; Zhang, C. The Hazards Analysis of Nickel-Rich Lithium-Ion Battery Thermal Runaway under Different States of Charge. *Electronics* **2021**, *10*, 2376. [[CrossRef](#)]
18. Yuan, W.; Jeong, S.; Sean, W.; Chiang, Y. Development of Enhancing Battery Management for Reusing Automotive Lithium-Ion Battery. *Energies* **2020**, *13*, 3306. [[CrossRef](#)]
19. Wu, L.; Pang, H.; Geng, Y.; Liu, X.; Liu, J.; Liu, K. Low-complexity state of charge and anode potential prediction for lithium-ion batteries using a simplified electrochemical model-based observer under variable load condition. *Int. J. Energy Res.* **2022**, *46*, 11834–11848. [[CrossRef](#)]
20. Armand, M.; Axmann, P.; Bresser, D.; Copley, M.; Edström, K.; Ekberg, C.; Guyomard, D.; Lestriez, B.; Novák, P.; Petranikova, M. Lithium-ion batteries—Current state of the art and anticipated developments. *J. Power Sources* **2020**, *479*, 228708. [[CrossRef](#)]
21. Li, Y.; Vilathgamuwa, M.; Xiong, B.; Tang, J.; Su, Y.; Wang, Y. Design of minimum cost degradation-conscious lithium-ion battery energy storage system to achieve renewable power dispatchability. *Appl. Energy* **2020**, *260*, 114282. [[CrossRef](#)]
22. Chen, T.; Jin, Y.; Lv, H.; Yang, A.; Liu, M.; Chen, B.; Xie, Y.; Chen, Q. Applications of lithium-ion batteries in grid-scale energy storage systems. *Trans. Tianjin Univ.* **2020**, *26*, 208–217. [[CrossRef](#)]
23. Wang, Q.; Shen, J.; He, Y.; Ma, Z. Design and management of lithium-ion batteries: A perspective from modeling, simulation, and optimization. *Chin. Phys. B* **2020**, *29*, 068201. [[CrossRef](#)]
24. Li, J.; Ye, M.; Jiao, S.; Meng, W.; Xu, X. A Novel State Estimation Approach Based on Adaptive Unscented Kalman Filter for Electric Vehicles. *IEEE Access* **2020**, *8*, 185629–185637. [[CrossRef](#)]
25. Guo, F.; Hu, G.; Xiang, S.; Zhou, P.; Hong, R.; Xiong, N. A multi-scale parameter adaptive method for state of charge and parameter estimation of lithium-ion batteries using dual Kalman filters. *Energy* **2019**, *178*, 79–88. [[CrossRef](#)]
26. Wang, Z.; Gladwin, D.T.; Smith, M.J.; Haass, S. Practical state estimation using Kalman filter methods for large-scale battery systems. *Appl. Energy* **2021**, *294*, 117022. [[CrossRef](#)]
27. Jiang, Z.; Li, H.; Qu, Z.; Zhang, J. Recent progress in lithium-ion battery thermal management for a wide range of temperature and abuse conditions. *Int. J. Hydrogen Energy* **2022**, *47*, 9428–9459. [[CrossRef](#)]
28. Feng, F.; Teng, S.; Liu, K.; Xie, J.; Xie, Y.; Liu, B.; Li, K. Co-estimation of lithium-ion battery state of charge and state of temperature based on a hybrid electrochemical-thermal-neural-network model. *J. Power Sources* **2020**, *455*, 227935. [[CrossRef](#)]

29. Shi, Y.; Ahmad, S.; Liu, H.; Lau, K.T.; Zhao, J. Optimization of air-cooling technology for LiFePO₄ battery pack based on deep learning. *J. Power Sources* **2021**, *497*, 229894. [[CrossRef](#)]
30. Yetik, O.; Karakoc, T.H. Estimation of thermal effect of different busbars materials on prismatic Li-ion batteries based on artificial neural networks. *J. Energy Storage* **2021**, *38*, 102543. [[CrossRef](#)]
31. Zhang, C.; Jiang, J.; Gao, Y.; Zhang, W.; Liu, Q.; Hu, X. Charging optimization in lithium-ion batteries based on temperature rise and charge time. *Appl. Energy* **2017**, *194*, 569–577. [[CrossRef](#)]
32. Corno, M.; Pozzato, G. Active adaptive battery aging management for electric vehicles. *IEEE Trans. Veh. Technol.* **2019**, *69*, 258–269. [[CrossRef](#)]
33. Castaings, A.; Lhomme, W.; Trigui, R.; Bouscayrol, A. Energy management of a multi-source vehicle by λ -control. *Appl. Sci.* **2020**, *10*, 6541. [[CrossRef](#)]
34. Eckert, J.J.; Silva, L.C.; Dedini, F.G.; Correa, F.C. Electric Vehicle Powertrain and Fuzzy Control Multi-objective Optimization, considering Dual Hybrid Energy Storage Systems. *IEEE Trans. Veh. Technol.* **2020**, *69*, 3773–3782. [[CrossRef](#)]
35. Vidal, C.; Malysz, P.; Kollmeyer, P.; Emadi, A. Machine learning applied to electrified vehicle battery state of charge and state of health estimation: State-of-the-art. *IEEE Access* **2020**, *8*, 52796–52814. [[CrossRef](#)]
36. Stroe, D.I.; Schaltz, E. Lithium-Ion Battery State-of-Health Estimation Using the Incremental Capacity Analysis Technique. *IEEE Trans. Ind. Appl.* **2020**, *56*, 678–685. [[CrossRef](#)]
37. Fotouhi, A.; Auger, D.J.; Propp, K.; Longo, S. Lithium–Sulfur Battery State-of-Charge Observability Analysis and Estimation. *IEEE Trans. Power Electron.* **2018**, *33*, 5847–5859. [[CrossRef](#)]
38. Benveniste, G.; Rallo, H.; Canals, L.; Merino, A.; Amante, B. Comparison of the state of lithium-sulphur and lithium-ion batteries applied to electromobility. *J. Environ. Manag.* **2018**, *226*, 1–12. [[CrossRef](#)] [[PubMed](#)]
39. Eckert, J.J.; Barbosa, T.P.; da Silva, S.F.; Silva, F.L.; Silva, L.C.; Dedini, F.G. Electric hydraulic hybrid vehicle powertrain design and optimization-based power distribution control to extend driving range and battery life cycle. *Energy Convers. Manag.* **2022**, *252*, 115094. [[CrossRef](#)]
40. Castanho, D.; Guerreiro, M.; Silva, L.; Eckert, J.; Antonini Alves, T.; Tadano, Y.d.S.; Stevan, S.L., Jr.; Siqueira, H.V.; Corrêa, F.C. Method for SoC Estimation in Lithium-Ion Batteries Based on Multiple Linear Regression and Particle Swarm Optimization. *Energies* **2022**, *15*, 6881. [[CrossRef](#)]
41. Zerrahn, A.; Schill, W.-P.; Kemfert, C. On the economics of electrical storage for variable renewable energy sources. *Eur. Econ. Rev.* **2018**, *108*, 259–279. [[CrossRef](#)]
42. Omariba, Z.B.; Zhang, L.; Kang, H.; Sun, D. Parameter Identification and State Estimation of Lithium-Ion Batteries for Electric Vehicles with Vibration and Temperature Dynamics. *World Electr. Veh. J.* **2020**, *11*, 50. [[CrossRef](#)]
43. Chen, Q.; Jiang, J.; Ruan, H.; Zhang, C. Simply designed and universal sliding mode observer for the SOC estimation of lithium-ion batteries. *IET Power Electron.* **2017**, *10*, 697–705. [[CrossRef](#)]
44. Li, S.; Li, G.; Ma, X. Grey prediction of lithium battery lifetime based on Markov rolling optimization. *J. Hefei Univ. Technol. Nat. Sci.* **2019**, *42*, 763–769.
45. Liu, S.; Dang, Y.; Fang, Z.; Xie, N. *Grey System Theory and Its Application*, 5th ed.; Science Press: Beijing, China, 2010.
46. Duan, H.; Wang, D.; Pang, X.; Liu, Y.; Zeng, S. A novel forecasting approach based on Multi-Kernel Nonlinear Multivariable Grey Model: A case report. *J. Clean. Prod.* **2020**, *260*, 120929. [[CrossRef](#)]
47. Wei, H.; Chen, X.; Lv, Z.; Wang, Z.; Pan, H.; Chen, L. Online Estimation of Lithium-Ion Battery State of Health Using Grey Neural Network. *Power Syst. Technol.* **2017**, *41*, 4038–4044.
48. Wu, W.; Ma, X.; Wang, Y.; Cai, W.; Zeng, B. Predicting China’s energy consumption using a novel grey Riccati model. *Appl. Soft Comput.* **2020**, *95*, 106555. [[CrossRef](#)]
49. Liu, Y.; Wu, Z.X.; Zhou, H.; Zheng, H.; Yu, N.; An, X.P.; Li, J.Y.; Li, M.L. Development of China Light-Duty Vehicle Test Cycle. *Int. J. Automot. Technol.* **2020**, *21*, 1233–1246. [[CrossRef](#)]
50. Liu, Y.; Zhou, H.; Xu, Y.; Qin, K.; Yu, H. *Feasibility Study of Using WLTC for Fuel Consumption Certification of Chinese Light-Duty Vehicles*; SAE International: Warrendale, PA, USA, 2018.
51. Tucki, K. A Computer Tool for Modelling CO₂ Emissions in Driving Cycles for Spark Ignition Engines Powered by Biofuels. *Energies* **2021**, *14*, 1400. [[CrossRef](#)]
52. Deng, Z.; Hu, X.; Lin, X.; Che, Y.; Xu, L.; Guo, W. Data-driven state of charge estimation for lithium-ion battery packs based on Gaussian process regression. *Energy* **2020**, *205*, 118000. [[CrossRef](#)]
53. Plett, G.L. Extended Kalman filtering for battery management systems of LiPB-based HEV battery packs: Part 3. State and parameter estimation. *J. Power Sources* **2004**, *134*, 277–292. [[CrossRef](#)]
54. Deng, Z.; Yang, L.; Cai, Y.; Deng, H.; Sun, L. Online available capacity prediction and state of charge estimation based on advanced data-driven algorithms for lithium iron phosphate battery. *Energy* **2016**, *112*, 469–480. [[CrossRef](#)]
55. Wang, L. Research on Reliability Predication and Life Cycle Cost Assessment of Low-voltage Switchgear. Ph.D. Thesis, Hebei University of Technology, Tianjin, China, 2017.